Available online at www.sciencedirect.com

ScienceDirect

Proceedings of the Combustion Institute xxx (2014) xxx–xxx

Proceedings of the Combustion Institute

www.elsevier.com/locate/proci

Weak and strong ignition of hydrogen/oxygen mixtures in shock-tube systems

Kevin P. Grogan, Matthias Ihme *

Department of Mechanical Engineering, Stanford University, Stanford, CA 94305, United States

Abstract

Detailed simulations of hydrogen/oxygen mixtures are performed to study weak and strong ignition regimes in a shock-tube system. An adaptive mesh refinement (AMR) algorithm in conjunction with a detailed chemistry representation is used to resolve physically relevant features such as the viscous boundary layer, the shock bifurcation region, and ignition kernels. The simulations employ a second-order accurate Navier–Stokes equations solver that is modified to include finite-rate reaction chemistry, wall-heat transfer, and detailed mass, thermal, and viscous-diffusion-transport properties. The operating conditions considered in this study span the thermodynamic state-space in the weak and strong ignition regimes. The treatment of wall-heat transfer is found to significantly alter the characteristics of ignition. The computations show that the mixing of the thermally stratified fluid, which carries different momentum and enthalpy, introduces inhomogeneities in the core region behind the reflected shock. These inhomogeneities act as localized ignition kernels. During the induction period, these kernels slowly expand and eventually transition to a detonation wave, rapidly consuming the unburned mixture. Effects of the reaction chemistry on the ignition behavior are examined by considering two different reaction mechanisms. A detailed analysis is performed to show that the transition from ignition kernel to detonation is well described by the SWACER mechanism.

Keywords: Shock-tube; Weak ignition; Heat transfer; SWACER; DDT

1. Introduction

Accurate chemical kinetic models are pivotal for characterizing effects of new fuel compositions on existing propulsion systems and for developing future combustion technologies. Shock-tube facilities remain invaluable in providing detailed information about ignition delay times, extinction limits, and species time histories for the development and validation of reaction mechanisms. In its simplest form, a shock-tube consists of a constant diameter pipe, which is divided into a driver section and a driven section by a diaphragm. The driver section is pressurized with an inert gas, and the driven section contains the test gas mixture that is under experimental investigation. Following the

* Corresponding author. Address: Department of Mechanical Engineering, Stanford University, 488 Escondido Mall, Stanford, CA 94305-3024, United States. Fax: +1 650 725 3525.

E-mail addresses: kgrogan@stanford.edu (K.P. Grogan), mihme@stanford.edu (M. Ihme).

http://dx.doi.org/10.1016/j.proci.2014.07.074

rupture of the diaphragm, a normal shock develops, which propagates into the driven section and is reflected off the end wall. Under ideal conditions, the test-gas mixture in the region behind the reflected shock is stationary and uniform. While this condition is ideal for chemical kinetics investigations, practical shock-tube systems are affected by non-idealities. Over recent years, several sources responsible for non-ideal shock-tube behaviors have been identified, including boundary layer growth [1,2], reflected shock/boundary layer interactions [3–5], and inhomogeneous ignition and weak-to-strong ignition transition [6–8]. The direct consequence of these non-idealities is increasing uncertainties in measurements, resulting in potential errors in derived rate coefficients and ignition delay times [9].

The state behind the reflected shock is of particular interest to the shock-tube community. In realistic systems, the reflected shock interacts with the boundary layer that develops behind the incident shock. Under certain conditions, shock bifurcation occurs and temperature inhomogeneities are introduced in the post-reflected shock region. The change in temperature due to the growth of the boundary layer has a significant effect on the measurements of ignition delay times and activation energies, and can result in systematic errors in excess of 20–40% [1,10]. For practical applications, boundary-layer effects can be partially mitigated by employing large shock-tube diameters and by reducing the test time [10]. However, if the operating range is extended to higher conversion rates, higher pressures, and longer ignition delay times, these hydrodynamic effects could increase in importance and may affect the experimental accuracy. Therefore, effects of the boundary layer on the conditions behind the reflected shock represent a limiting factor toward extending the shock-tube performance to longer operating conditions.

Simple models such as Chemshock [11] and the VTIM (volume as a function of time) reactor model [6] have been developed to consider effects of the pressure rise of realistic shock-tube systems in homogeneous reactor models. By incorporating pressure measurements into zero-dimensional simulations, these models were found to improve the agreement with experimental data; however, they only provide an incomplete description of the gas-dynamics in a shock-tube within the weak ignition regime.

The objective of this work is to examine effects of the shock bifurcation, wall conditions, and operating regimes on the flow-field and ignition dynamics in the region behind the reflected shock. To this end, detailed simulations are conducted in order to quantify direct contributions of these non-ideal processes on the ignition behavior in the shock-reflected region.

The remainder of this paper is organized as follows: a description of the relevant physics of weak ignition is summarized in the next section. The mathematical model is presented in Section 3. Simulation results are discussed in Section 4, in which effects of boundary conditions, operating conditions, transition mechanisms, and the reaction chemistry are analyzed. The paper finishes with conclusions.

2. Ignition physics in shock-tube systems

Weak and strong ignition: Of interest to the present investigation is the weak and strong ignition behavior of H_2/O_2-mixtures. Weak ignition is a combustion phenomenon that is observed for certain operating conditions, and is associated with the non-uniform and distributed ignition of the mixture. This is in contrast to strong ignition, in which a wave is initiated by autoignition at the end wall of the shock-tube and propagates through the mixture.

Voevodsky and Soloukhin [12] first studied weak and strong ignition processes experimentally by considering a stoichiometric H_2/O_2-mixture in a shock-tube system. By excluding side-wall effects and vibrational relaxation processes, they attributed the presence of the weak ignition to a kinetic phenomenon that is demarcated by the second explosion limit. Meyer and Oppenheim [8] correlated the occurrence of weak ignition events to the sensitivity of the ignition delay time with respect to the post-reflected shock temperature. For stoichiometric H_2/O_2-mixtures they deduced the strong ignition limit using the following empirical relation [8]:

$$\left.\frac{\partial \tau_{\text{ign}}}{\partial T_5}\right|_{p_5} = -2\ (\mu\text{s/K}), \tag{1}$$

where τ_{ign} is the ignition delay time, and T_5 and p_5 are the temperature and pressure in the reflected shock region, respectively. Meyer and Oppenheim concluded that weak ignition is a gas-dynamic phenomenon that is induced by perturbations to the flow-field.

Experimental data [8,12] for weak and strong ignition of stoichiometric H_2/O_2-mixtures together with hydrogen explosion limits, and the sensitivity criterion of Eq. (1) are presented in Fig. 1. The sensitivity criterion due to Meyer and Oppenheim (dashed line) is shown to perform slightly better in predicting the weak ignition boundary than the second explosion limit – particularly in the low pressure region between the two curves. In Section 4, we examine the ignition criterion through simulations and the nominal operating points for the simulations are indicated by triangles in Fig. 1.

Shock bifurcation: A shock bifurcation is formed when a reflected shock interacts with the low momentum boundary layer that is developed behind the incident shock as it propagates toward

Please cite this article in press as: K.P. Grogan, M. Ihme, *Proc. Combust. Inst.* (2014), http://dx.doi.org/10.1016/j.proci.2014.07.074

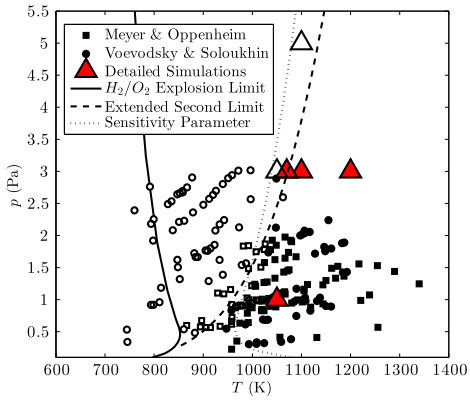

Fig. 1. Weak and strong ignition delineations as a function of temperature and pressure; open symbols denote weak ignition while closed symbols indicate strong ignition events. Explosion limit and extended second limit were obtained from Lewis and von Elbe [35], and the sensitivity parameter was evaluated using the correlation due to Meyer and Oppenheim [8].

the end wall [3]. Due to differences in pressure and entropy across the reflected shock and the bifurcation region, a high momentum jet develops as the boundary layer fluid is deflected and passes under the oblique shock. As the boundary layer is consumed by the reflected shock, the adverse pressure gradient across the bifurcation causes it to separate and eventually stagnate. The entrainment of fluid through the bifurcation foot results in a continuous growth of the triple-shock structure. The continuous entrainment of the boundary layer increases the size of the interaction zone, thereby enhancing the mixing in the region behind the reflected shock. As the fluid is ejected from the tail shock, a shear layer develops between the shock-compressed and colder boundary layer fluids. This leads to the formation of a slip line that is hydrodynamically unstable as noted by Weber et al. [13], promoting the mixing between the different fluids.

Detonation transition: Shock Wave Amplification by Coherent Energy Release (SWACER) [14,15] is a mechanism that explains the transition of isolated ignition kernels to a detonation structure. The SWACER theory predicts a spontaneous transition into a detonation wave if there is a coherent coupling of pressure oscillations and heat release at the ignition kernel [16]. The transition criterion is given as:

$$\zeta = a\frac{dT}{dx}\frac{d\tau_{\text{ign}}}{dT} = \mathcal{O}(1), \tag{2}$$

where ζ is the non-dimensional SWACER parameter, and a is the sound speed. Gu et al. [17] studied the flame kernel transition in one-dimensional simulations and found acceptable agreement between Eq. (2) and observed detonation transition. As will be examined in Section 4, the SWACER mechanism is postulated to induce transition from flame kernels into detonation fronts as a mode of weak ignition in shock-tubes.

3. Mathematical model, computational setup, and operating conditions

In this study, we consider the end of the driven section of a shock-tube with an inner diameter R. Using classical boundary layer scaling, it can be shown that curvature effects can be neglected for the conditions that $(R/\delta - 1)^{-1} \ll 1$. By estimating the boundary layer thickness δ using Mirel's similarity solution [18] it is found that this term is of order $\mathcal{O}(10^{-2})$ for all flow conditions examined in this work. With this, we consider the spatio-temporal evolution of the flow, ignition, and combustion inside a planar shock-tube. The governing equations are the reactive Navier–Stokes equations, which are here written in index form as [19]:

$$\frac{\partial \mathbf{U}}{\partial t} + \frac{\partial}{\partial x_j}\left(\mathbf{F}_j^c - \mathbf{F}_j^v\right) = \mathbf{S}, \tag{3}$$

where $\mathbf{U}$ is the state vector, $\mathbf{F}_j^c$ and $\mathbf{F}_j^v$ are the convective and viscous fluxes, and $\mathbf{S}$ is the source term vector. These quantities have the following definition:

$$\mathbf{U} = (\rho u_i, \rho e_t, \rho Y_n)^T, \tag{4a}$$

$$\mathbf{F}_j^c = (\rho u_j u_i + p\delta_{ij}, u_j(\rho e_t + p), \rho Y_n u_j)^T, \tag{4b}$$

$$\mathbf{F}_j^v = (\tau_{ij}, u_i\tau_{ij} + q_j, \rho Y_n V_{jn})^T, \tag{4c}$$

$$\mathbf{S} = (0_i, 0, \dot{\omega}_n)^T, \tag{4d}$$

for $\{i,j\} = 1,\ldots,N_D$ and $n = 1,\ldots,N_S$, where N_D denotes the spatial dimension, and N_S is the number of chemical species. The total internal energy is denoted by e_t, τ_{ij} is the viscous stress tensor using Stokes' hypothesis, V_{jn} is the diffusion velocity of species n, $\dot{\omega}_n$ is the chemical source term of species n, q_i is the heat-flux vector, and the mass diffusion is described by a multi-component diffusion model with thermal and pressure diffusion. The dynamic viscosity of the mixture is obtained using a modified Wilke mixing rule [20], the thermal conductivity is found using Mathur's mixing rule [21], and the ideal gas law is used as the state equation.

The governing equations are solved using a block-structured adaptive mesh refinement (AMR) method, which is implemented in the object-oriented framework AMROC (Adaptive Mesh Refinement in Objective-oriented C++) [22,23]. All spatial operators are discretized using a second-order accurate finite-volume discretization, a forward Euler method is used for the temporal integration, and a van Albada limiter [24] is used to capture shocks and contact discontinuities. Instead of simulating the entire shock-tube, in this

Please cite this article in press as: K.P. Grogan, M. Ihme, *Proc. Combust. Inst.* (2014), http://dx.doi.org/10.1016/j.proci.2014.07.074

study we only consider the end section of the shock-tube. The computational domain consists of a symmetric two-dimensional planar shock-tube, having a length of either 10 or 20 cm, and a radius of either 1.0 or 2.5 cm.

The length of the domain in all cases is sufficient to contain the shock bifurcation for the entirety of the simulation until ignition. The radius is varied to study the effect of the shock-tube diameter on ignition. The computational mesh consists of square cells with a minimum grid size of 3.125 μm in the most resolved case, corresponding to an equivalent number of grid cells of approximately 205 million or approximately ten cells per Chapman–Jouguet detonation induction length for a stoichiometric hydrogen oxygen mixture. Four levels of adaptive mesh refinement are used to ensure that all physical processes in smoothly varying regions are properly resolved. For this grid resolution, no substantial differences in the formation of ignition kernels are found by further refining the mesh. The reaction chemistry is described by the high-pressure H_2/O_2 kinetic model of Li et al. [25], consisting of $N_S = 13$ species among 25 chemical reactions. Additionally, the mechanism due to Hong et al. [26] is used for comparison.

The following boundary and initial conditions are employed: along the centerline, symmetric boundary conditions are prescribed, and walls at the top and right end of the driven section are described using adiabatic or isothermal no-slip boundary conditions. In the case of isothermal wall simulations, the wall temperature is set to 304 K. The flow-field is initialized by a moving shock using normal-shock relations, and the initial shock strength and conditions in the driven section are prescribed to obtain target conditions in the region behind the reflected shock (region 5). All simulations are initiated at a sufficient distance away from the end wall to ensure boundary layer development.

4. Results

Several configurations are examined and are summarized in Table 1. In the order of presentation, Case 2 examines the effect of the heat transfer at the boundaries on the ignition behavior, Cases 1–4 span the thermodynamic state-space to examine the veracity of the postulated ignition regime demarcations, Case 3 investigates the dependence of ignition delay on diameter size, Case 5 allows us to study a transition mode from deflagration-to-detonation via the SWACER-mechanism as well as the mean thermo-chemical properties within an ignition kernel, and Case 6 examines the effects of the different chemical mechanisms on the ignition.

4.1. Effects of thermal boundary conditions on ignition behavior

Both isothermal and adiabatic wall boundary conditions were employed in previous computational studies of shock bifurcation and weak ignition phenomenon [27,28,13]. In the present work, two simulations are performed to examine the differences due to the treatment of heat transfer at the wall. For these simulations a stoichiometric H_2/O_2 mixture is considered under nominal conditions $T_5 = 1070$ K and $p_5 = 3 \times 10^5$ Pa, corresponding to Case 2 in Table 1.

Differences in the ignition behavior as a result of the different wall-boundary conditions are presented in Fig. 2. Case 2a–w (Fig. 2(a)) shows that the ignition first occurs in the stagnation region of the bifurcation foot. This ignition kernel expands spatially along the boundary layer. At time $t = 60$ μs the spontaneous formation of three ignition kernels at the centerline can be observed. These kernels form due to the raised temperature along the centerline immediately following the shock. As described by Mark [3], the temperature increase near the normal shock is due to an isentropic nozzle effect in which the fluid expands as the shock bifurcation passes. Additionally, pressure waves from the ignited boundary layer fluid are shown to perturb the bulk fluid. This causes an acceleration of the reaction chemistry allowing for hot-spot ignition. In contrast, the simulation with isothermal boundary conditions (Case 2i-s in Fig. 2(b), shows strong ignition, which is initiated a short distance away from the end wall.

The cause of the discrepancy between the two cases is due to the increased temperature in the boundary layer as a result of viscous dissipation effects for the adiabatic simulation. This causes the mixture in the stagnation bubble to ignite; consequently, the fluid volumetrically expands and accelerates. The thermal expansion intensifies the shear layer between the two fluids and enlarges the shock-foot height. The decrease in shock-foot height due to heat transfer from the side wall agrees with the findings of Weber et al. [13]. Additionally, a comparison of the shock-foot height with the empirical correlation by Peterson and Hanson [29] shows agreement to within 2% for the 5 cm diameter case; however, the simulations deviate from the empirical correlation by over 10% for the 2 cm diameter cases.

Due to the weak ignition, shown in Fig. 2(a), Case 2a–w predicts an ignition delay of 47 μs in contrast to the isothermal case, which predicts an ignition delay of 75 μs (time is measured with respect to the reflection of the shock at the end wall).

Shock-tubes are traditionally modeled assuming adiabaticity and an isochoric process (constant UV) [6]. However, the evaluated ignition delay times for both simulations differ significantly from

Please cite this article in press as: K.P. Grogan, M. Ihme, *Proc. Combust. Inst.* (2014), http://dx.doi.org/10.1016/j.proci.2014.07.074

Table 1
Operating conditions for the shock-tube investigations. $(T,p)_5$ denotes the target condition of the shock-reflected mixture in (K, bar); R is the radius, in cm; adiabatic/isothermal wall boundary conditions; Li/Hong mechanism; and weak/strong ignition. Refer to Fig. 1 for representation in the state-space diagram for all cases.

Case	Mixture composition	$(T,p)_5$	R	B.C.	Mech.	Ign.
1	H_2:O_2 = 2:1	(1200,3)	1.0	i	L	s
2	H_2:O_2 = 2:1	(1070,3)	1.0	a/i	L	w/s
3	H_2:O_2 = 2:1	(1050,3)	1.0/2.5	i	L	w
4	H_2:O_2 = 2:1	(1050,1)	1.0	i	L	s
5	H_2:O_2:Ar = 15:17.15:67.85	(1100,5)	1.0	i	L	w
6	H_2:O_2 = 2:1	(1100,3)	1.0	i	L/H	s/w

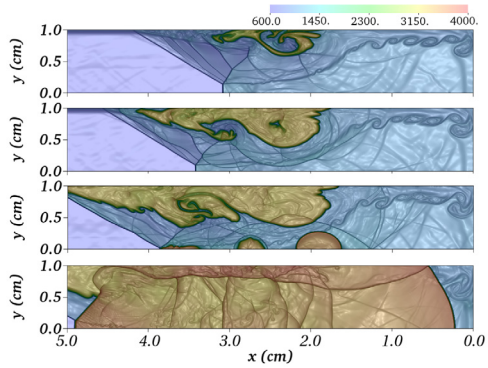

(a) Case 2a-w: Adiabatic wall, weak ignition.

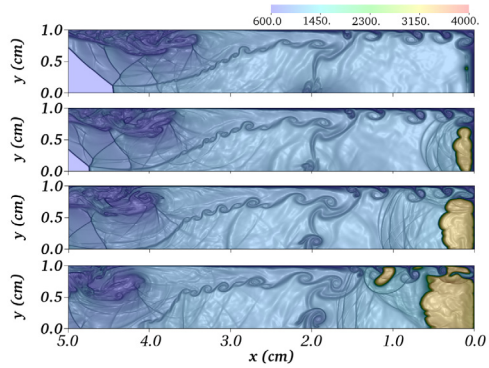

(b) Case 2i-s: Isothermal wall, strong ignition.

Fig. 2. Transient evolution of the temperature field during the ignition process, separated by 5 μs increments starting at 50 and 74 μs for (a) adiabatic and (b) isothermal wall conditions, respectively. Nominal conditions for both cases are $T_5 = 1070$ K and $p_5 = 3$ bar. The magnitude of the temperature gradients is overlaid.

those of a constant UV reactor by 27% and 17% for the adiabatic and isothermal cases, respectively. This suggests that effects of gas-dynamic inhomogeneities can lead to significant discrepancies in ignition delay within this regime for both configurations.

Following Mark's analysis [3], the rise in the wall temperature ΔT_w due to the heat transfer from the gas can be estimated as:

$$\Delta T_w = \Delta T_s \sqrt{\frac{(\lambda \rho c_p)_{gas}}{(\lambda \rho c)_w}}, \tag{5}$$

where ΔT_s is the temperature rise across the shock, and λ is the heat conductivity. Using values obtained from the simulation for the fluid at the wall and representative values for the shock-tube wall assumed to be made of stainless steel, the temperature rise at the wall is estimated to be 0.3 K. Hence, the isothermal boundary conditions are considered to be physically more representative and are employed for subsequent calculations.

4.2. Examination of weak and strong ignition behavior

Figure 1 summarizes representative weak and strong ignition measurements for stoichiometric H_2/O_2-mixtures as a function of temperature and pressure. Additionally, the ignition criterion by Meyer and Oppenheim, given by Eq. (1) is shown. This criterion is empirically derived to fit experimental data. As such, this criterion is only applicable to non-diluted, stoichiometric H_2/O_2 mixtures, and mixtures with different compositions must be evaluated independently. From the experimental data shown in Fig. 1, five conditions are selected to span the thermodynamic state space of stoichiometric H_2/O_2 mixtures near the weak ignition limit given by Meyer and Oppenheim. These are Cases 1–4 shown in Table 1.

Weak ignition is shown in Fig. 3 for two different shock-tube diameters. These results show that the longer ignition delay allows for a pronounced bifurcation structure to develop. Additionally, the high-speed shear layer trailing the bifurcation is shown to cause significant mixing, which introduces inhomogeneities into the stagnation region behind the reflected shock. Consequently, a hot-spot ignition kernel is shown to develop immediately following the shock front.

As shown in Fig. 3(a), the shock bifurcation has grown to the radius of the tube at the end of the simulation; this introduces significant inhomogeneities into the flow-field. To examine effects of

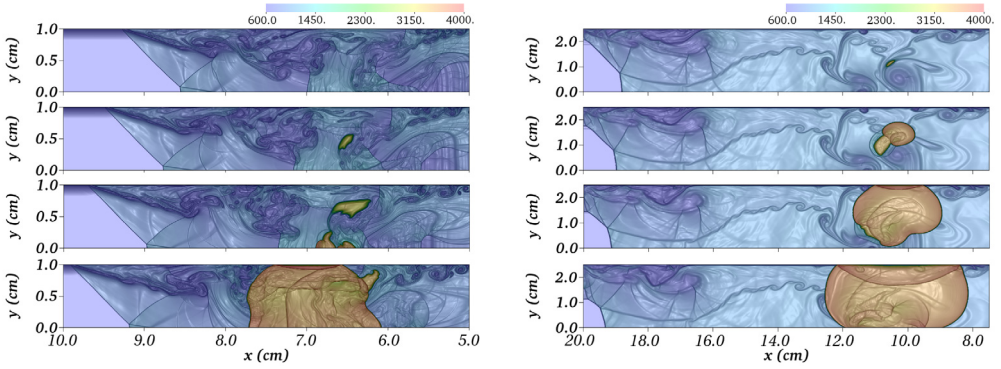

(a) Case 3i-w with R = 1 cm. (b) Case 3i-w with R = 2.5 cm.

Fig. 3. Transient evolution of the temperature field during the ignition process in 3 μs increments starting at 213 and 323 μs for (a) small (1.0 cm) radius and (b) large (2.5 cm) radius conditions, respectively. Both cases had nominal conditions $T_5 = 1050$ K and $p_5 = 3$ bar. The magnitude of the temperature gradients is overlaid.

the shock-tube diameter on the bifurcation and ignition as well as to approach more realistic tube diameters used in shock-tube studies, an additional simulation at the same nominal thermodynamic conditions but at a radius of $R = 2.5$ cm is undertaken. This size is selected such that the bifurcation would not intercept the symmetry plane for the duration of the simulation. The temporal evolution of the temperature field post-ignition is shown in Fig. 3(b). The kernel formation, obtained from the simulation, is characteristic of weak ignition; however, the mixture in the large diameter case ignites 108 μs *after* that observed for the case with $R = 1$ cm. Additionally, the ignition time in the large diameter case corresponds well to the ignition delay of a homogeneous UV reactor with just 3% difference while in the small diameter case the ignition time differs by 31% with the homogeneous UV reactor. These results demonstrate that the shock-tube diameter has a significant effect on the measured ignition delay, and this sensitivity increases with increasing ignition delay times.

As shown in Fig. 1, the detailed simulations show good correspondence with the ignition criterion due to Meyer and Oppenheim. However, the demarcation between weak and strong ignition is both mixture- and facility-dependent as the shock-tube geometry can significantly exacerbate weak ignition phenomena.

4.3. Mechanism for flame kernel transition to detonation

The modes of kernel formation and weak ignition were studied by Blumenthal et al. [7]. Different modes in which a deflagration wave may transition into a detonation within a shock-tube include:

- A deflagration originating near the end wall undergoes classical deflagration-to-detonation transition, in which pressure waves released by the deflagration preconditions the unburnt mixture, accelerating the deflagration until transition to detonation occurs.
- A flame kernel produces pressure waves that coherently build up with the reaction front, thereby inducing transition to detonation (SWACER mechanism).
- Flame kernels interact with other kernels or walls to strengthen the reaction front causing transition.

To investigate the flame-kernel transition, an operating condition is selected that is consistent with the experimental investigations by Blumenthal et al. [7]. This condition corresponds to the Argon-diluted H_2/O_2-mixture of Case 5. Our simulations confirm weak ignition. Specifically, ignition is initiated by the formation of a cylindrical ignition kernel near the end wall of the shock-tube, which transitions into a detonation wave. The transition process from ignition kernel to detonation is illustrated in Fig. 4.

The simulation data depicted in Fig. 4 were reduced by averaging across annular cross-sections around the ignition kernel, and the location of the ignition center was found by fitting a Gaussian curve to the temperature data just after ignition. As shown in Fig. 4, the ignition kernel originated from a slight perturbation in the temperature-field, which is approximately 5 K above the surrounding. As the locus of the kernel becomes fully reacted the reaction front begins to move outward. When the reaction front is at approximately 0.25 cm, the pressure wave, created by the front, became coherent with the outward propagation of the temperature front. This positive feedback strengthens the

Please cite this article in press as: K.P. Grogan, M. Ihme, *Proc. Combust. Inst.* (2014), http://dx.doi.org/10.1016/j.proci.2014.07.074

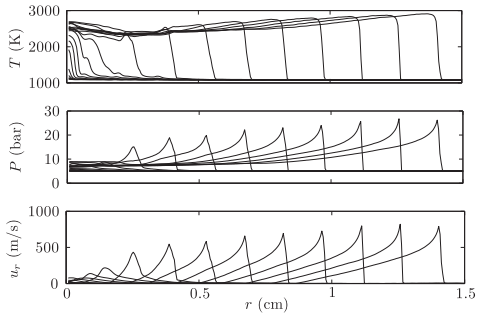

Fig. 4. Sequential plots at 1 μs time increments showing the ignition kernel transition to detonation for Case 5. Nominal conditions are $T_5 = 1100$ K and $p_5 = 5$ bar.

front until a detonation develops between 0.5 and 1 cm. The transition of the ignition kernel in Case 5 is well explained by the SWACER mechanism discussed in Section 2.

4.4. Comparison of reactor models

Figure 5 compares the thermochemistry of the kernel ignition to an isochoric (UV) and isobaric (HP) reactor. By comparison of the variation in density in the kernel ignition from the outset, it is shown that during the deflagration stage, the kernel ignition closely resembles an isobaric reactor. However, once the ignition kernel develops into a detonation, the ignition more closely resembles an isochoric reactor. This is expected when one considers the Hugoniot relation for a one-dimensional Rayleigh flow, where the pressure change is small for a deflagration and the density change is small for a detonation.

4.5. Evaluation of mechanism sensitivity

To examine the sensitivity of weak ignition to the reaction mechanism, additional simulations are performed using the mechanism due to Hong et al. [26]. The comparative sensitivity of the Li and Hong mechanism is shown in Fig. 6. The Hong mechanism is shown to have a peak sensitivity at approximately 1100 K in contrast to the Li mechanism, which is relatively insensitive under this condition. At the pressure condition under examination, the peak in the logarithmic sensitivity coefficient is found to correlate well with weak ignition. Additionally, the sensitivity of the kinetic model due to Burke et al. [30] is included in Fig. 6. Because of the comparable performance to the mechanism by Li et al., this kinetic model is not further considered for comparison through a detailed simulation.

As shown in Fig. 7, the mode of ignition for the Li mechanism is a planar homogeneous ignition, which transitioned to a detonation. In contrast, the Hong mechanism shows kernel

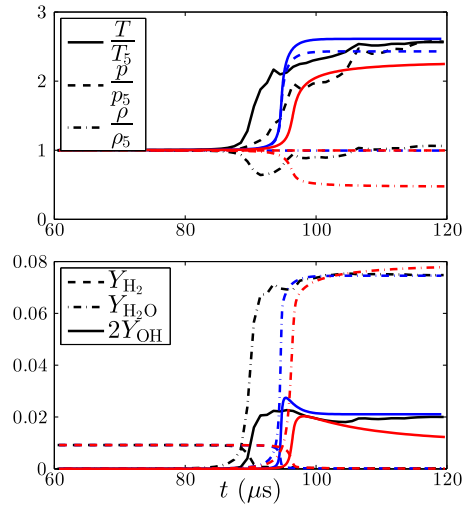

Fig. 5. Comparison of an ignition kernel to adiabatic isochoric (constant UV) and isobaric (constant HP) reactors. The kernel quantities are found by averaging up to the extent of the combustion wave determined by the maximum slope of the temperature. The kernel ignition data are taken from Case 5. The mean kernel quantities from the detailed simulation are shown in black, the isochoric reactor is shown in blue, and the isobaric reactor is shown in red. (For interpretation of the references to color in this figure caption, the reader is referred to the web version of this article.)

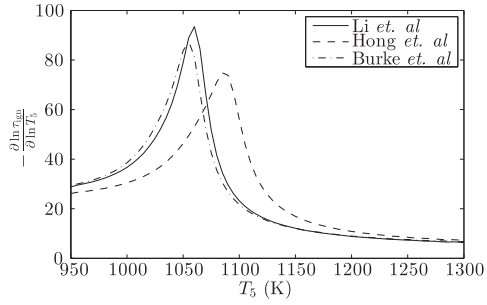

Fig. 6. Sensitivity of the mechanisms due to Li et al. [25], Hong et al. [26], and Burke et al. [30] at 3 bar.

formation brought about by a vortex that is shed by the slip line squeezing fluid in the bulk to form an ignition hotspot; subsequently, the ignition hotspot transitioned into a detonation. This vortex shedding from the slip line corresponded to that found by Ziegler [31]. Additionally, the location of the ignition kernel is shown to align with the triple-point trajectory in accordance to the experimental findings of Yamashita et al. [32]. From Fig. 7, it is manifested that the Li mechanism exhibits strong ignition while the Hong mechanism shows weak ignition.

The change in ignition mode due to the different mechanisms illustrates the importance of an

Please cite this article in press as: K.P. Grogan, M. Ihme, *Proc. Combust. Inst.* (2014), http://dx.doi.org/10.1016/j.proci.2014.07.074

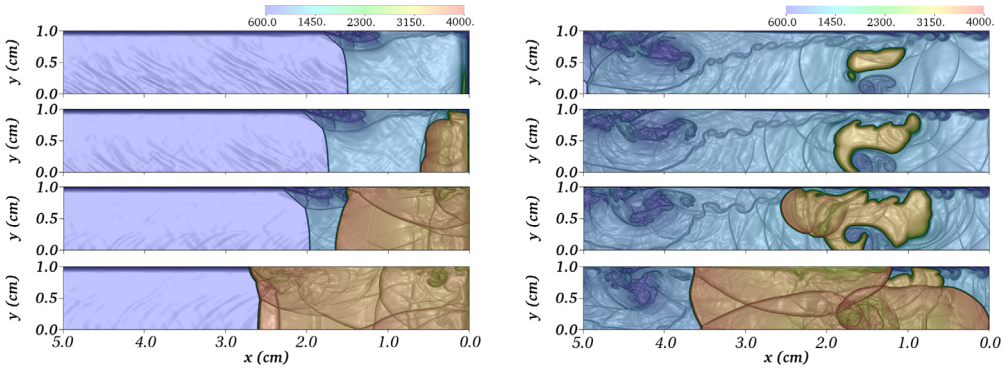

(a) Li Mechanism: Case 6L-s. (b) Hong Mechanism: Case 6H-w.

Fig. 7. Transient evolution of the temperature field during the ignition process in 4 μs increments starting at 26 and 82 μs for (a) the Li mechanism and (b) the Hong mechanism, respectively. Both cases have nominal conditions $T_5 = 1100$ K and $p_5 = 3$ bar. The magnitude of the temperature gradients is overlaid.

accurate chemical model for describing this chemically sensitive ignition regime. While the gas-dynamics produce the conditions required for kernel formation, the sensitivity of the chemical mechanism to the perturbation in the flow is shown to have severe consequences. Hence, these detailed simulations indicate that homogeneous reactor simulations alone are insufficient to describe the complex interaction between gas-dynamics and reaction chemistry, and spatially-resolved models are necessary to accurately represent ignition phenomena in this transition regime.

5. Conclusions

Simulations of ignition phenomena of hydrogen/oxygen mixtures in shock-tubes using detailed chemistry and diffusion are undertaken in this work. From these simulations, the following conclusions are drawn:

- The choice of thermal boundary conditions at the walls is shown to have a significant impact on the ignition mode in shock-tube simulations. The adiabatic boundary condition is shown to heat the boundary-layer fluid by viscous-dissipative effects, causing the boundary-layer fluid to ignite when stagnated behind the reflected shock wave. Isothermal boundary conditions are physically more justifiable considering the thermal properties of the mixture and the material properties of the shock-tube.
- The simulations show correspondence with the weak ignition criterion due to Meyer and Oppenheim. Weak ignition is demonstrated to be a gas-dynamic phenomenon brought about by perturbations to the ideally stagnant flow-field behind the reflected shock. The mechanism for weak ignition for all cases examined was the bifurcation of the reflected shock wave, introducing fluctuations in the flow-field via a high-velocity shear layer; this causes pockets of temperature inhomogeneities which accelerate the ignition process.
- A correspondence with the diameter of the shock-tube and weak ignition is found. By varying the radius of the shock-tube in the simulations, weak ignition is found to be mollified in the case with the larger diameter leading to an ignition delay close to that of a homogeneous reactor.
- The SWACER-mechanism is used to explain the transition of an ignition kernel from a deflagration to a detonation. By considering an Argon-diluted mixture, it is shown that ignition is initiated by the formation of a local hot-spot near the end wall of the shock-tube. The reaction front of the kernel moves at approximately the acoustic velocity of the mixture; this causes a coherence with the reaction front and the pressure waves released by the reaction, resulting in the formation of a detonation wave.
- Weak ignition is not found to be well-described by either an isochoric or an isobaric reactor. From the outset, the ignition kernel resembles an isobaric reactor in correspondence with a deflagration, but as the kernel transitions to a detonation, an isochoric reactor seems more appropriate. These findings suggest that a blending of the two reactor models may be useful when studying fuels in thermodynamic regimes prone to kernel formation and DDT.
- The ignition mode is shown to be sensitive to the chemical mechanism. This implies that zero-dimensional reactor models are insufficient to fully describe this highly sensitive regime, and the development of chemical

Please cite this article in press as: K.P. Grogan, M. Ihme, *Proc. Combust. Inst.* (2014), http://dx.doi.org/10.1016/j.proci.2014.07.074

mechanisms should be accompanied by spatial simulations to evaluate gas-dynamic effects in the weak ignition regime.

Other effects, arising from residual radical concentrations, mixture impurities, and turbulent flow-field fluctuations, have not been considered in this investigation [33,34]. These effects can play an equally important role in affecting the ignition behavior in shock-tube systems.

Acknowledgments

Financial support through the Air Force Office of Scientific Research under Award No. FA9550–11-1–0031 is gratefully acknowledged. We would also like to thank Ralf Deiterding for generously allowing us to use his code. This work made use of the Extreme Science and Engineering Discovery Environment (XSEDE), which is supported by National Science Foundation Grant No. ASC130004.

References

[1] R.L. Belford, R.A. Strehlow, *Ann. Rev. Phys. Chem.* 20 (1969) 247–272.
[2] E.L. Petersen, R.K. Hanson, *Shock Waves* 10 (2001) 405–420.
[3] H. Mark, *J. Aeronaut. Sci.* 24 (1957) 304–306.
[4] R.A. Strehlow, A. Cohen, *J. Chem. Phys.* 30 (1959) 257–265.
[5] M. Honda, K. Takayama, O. Onodera, Y. Kohama, Motion of reflected shock waves in shock tube, in: *Proc. of the 10th Intern. Shock Tube Symp.*, pp. 312–319, 1975.
[6] M. Chaos, F.L. Dryer, *Int. J. Chem. Kinet.* 42 (3) (2010) 143–150.
[7] R. Blumenthal, K. Fieweger, K.H. Komp, G. Adomeit, *Combust. Sci. Tech.* 113 (1996) 137–166.
[8] J.W. Meyer, A.K. Oppenheim, *Proc. Combust. Inst.* 13 (1971) 1153–1164.
[9] C.T. Bowman, R.K. Hanson, *J. Phys. Chem.* 83 (6) (1979) 757–763.
[10] D.F. Davidson, R.K. Hanson, *Shock Waves* 19 (2009) 271–283.
[11] H. Li, Z.C. Owens, D.F. Davidson, R.K. Hanson, *Int. J. Chem. Kinet.* (2009) 189–198.
[12] V.V. Voevodsky, R.I. Soloukhin, *Proc. Combust. Inst.* 10 (1965) 279–283.
[13] Y.S. Weber, E.S. Oran, J.P. Boris, J.D. Anderson, *Phys. Fluids* 7 (1995) 2475–2488.
[14] Y.B. Zeldovich, V.B. Librovich, G.M. Makhviladze, G.I. Sivashinsky, *Acta Astronautica* 15 (1970) 313–321.
[15] J.H. Lee, R. Knystautas, N. Yoshikawa, *Acta Astronautica* 5 (1978) 971–982.
[16] J.H.S. Lee, *The Detonation Phenomenon*, Cambridge University Press, Cambridge, 2008.
[17] X. Gu, D. Emerson, D. Bradley, *Combust. Flame* 133 (2003) 63–74.
[18] H. Mirels, Boundary Layer Behind Shock or Thin Expansion Wave Moving into Stationary Fluid, NACA TN 3721, Lewis Flight Propulsion Laboratory, Cleveland, OH, 1956.
[19] F.A. Williams, *Combustion Theory*. Perseus Books, Reading, MA, 1985.
[20] R.B. Bird, W.E. Stewart, E.N. Lightfoot, *Transport Phenomena*, 2nd ed., John Wiley & Sons, 2002.
[21] S. Mathur, P.K. Tondon, S.C. Saxena, *Mol. Phys.* 12 (6) (1967) 569–579.
[22] R. Deiterding. AMROC – Blockstructured Adaptive Mesh Refinement in Object-oriented C++. Available at <http://amroc.sourceforge.net>, 2008.
[23] R. Deiterding, *Detonation structure simulation with AMROC*, in: L.T. Yang, O.F. Rana, B. Martino, J. Dongarra (Eds.), *High Performance Computing and Communications, Lecture Notes in Computer Science*, Vol. 3726, Springer, Berlin Heidelberg, 2005, pp. 916–927.
[24] G.D. van Albada, B. van Leer, W.W. Roberts, *Astron. Astrophys.* 108 (1982) 76–84.
[25] J. Li, Z. Zhao, A. Kazakov, F.L. Dryer, *Int. J. Chem. Kinet.* 36 (10) (2004) 566–575.
[26] Z. Hong, D. Davidson, R. Hanson, *Combust. Flame* 158 (2011) 633–644.
[27] M. Ihme, Y. Sun, R. Deiterding, Detailed simulations of weak-to-strong ignition of a H_2/O_2/Ar mixture in shock-tubes, in: 29th International Symposium on Shock Waves, Madison, WI, July 14–19, 2013.
[28] A.M. Khokhlov, J.M. Austin, C. Bacon, S. Aithal, K. Riley, Reflected shock bifurcation in a square channel, AIAA Paper 2011-646, 2011.
[29] E.L. Peterson, R.K. Hanson, *Shock Waves* 15 (2006) 333–340.
[30] M.P. Burke, M. Chaos, Y. Ju, F.L. Dryer, S.J. Klippenstein, *Int. J. Chem. Kinet.* 44 (7) (2012) 444–474.
[31] J. Ziegler, Simulations of Compressible, Diffusive, Reactive Flows with Detailed Chemistry Using a High-Order Hybrid WENO-CD Scheme. PhD Thesis, California Institute of Technology, 2011.
[32] H. Yamashita, J. Kasahara, Y. Sugiyama, A. Matsuo, *Combust. Flame* 159 (2012) 2954–2966.
[33] J. Urzay, N. Kseib, D.F. Davidson, G. Iaccarino, R.K. Hanson, *Combust. Flame* 161 (1) (2014) 1–15.
[34] M. Ihme, *Combust. Flame* 159 (4) (2012) 1592–1604.
[35] B. Lewis, G. von Elbe, *Combustion, Flames, and Explosions of Gases*, Academic Press, 1987.